Journal of Applied Polymer Science

Preparation and property investigation of crosslinked alginate/silicon dioxide nanocomposite films

Manli Yang,[1,2,3] Yanzhi Xia,[1,3,4] Yingxia Wang,[1,3] Xihui Zhao,[1,3] Zhixin Xue,[1,3] Fengyu Quan,[1,3] Cunzhen Geng,[1,3] Zhihui Zhao[3,4]

[1]College of Chemistry and Chemical Engineering, Qingdao University, Qingdao 266071, People's Republic of China
[2]College of Chemistry and Pharmaceutical Science, Qingdao Agricultural University, Qingdao 266109, People's Republic of China
[3]Collaborative Innovation Center for Marine Biomass Fibers, Materials, and Textiles of Shandong Province, Qingdao University, Qingdao 266071, People's Republic of China
[4]State Key Laboratory Cultivating Base for New Fiber Materials and Modern Textiles, Qingdao University, Qingdao 266071, People's Republic of China
Correspondence to: Y. Xia (E-mail: xiayzh@qdu.edu.cn)

ABSTRACT: Crosslinked nanocomposite films of sodium alginate (SA) and silicon dioxide (SiO_2) with different SiO_2 loading values were prepared by *in situ* synthesis. Biocomposite films were produced by solution casting and solvent evaporation with glycerol as the plasticizer and calcium chloride as the crosslinking agent. The effects of the addition of nano silicon dioxide (nano-SiO_2) in SA on the microstructural, physical, mechanical, and optical properties of the nanocomposite films were characterized. The results show that nano-SiO_2 was dispersed homogeneously in the SA matrix; it thereby formed a strong interfacial interaction between the nano-SiO_2 particles and the matrix. The transparency of the bionanocomposite films was enhanced. Thermogravimetric analysis also revealed that nano-SiO_2 improved the thermal stability of the SA films. The incorporation of SiO_2 further reduced the water vapor permeability and swelling degree and significantly increased the tensile strength and elongation, which are parameters important for packaging industries. Finally, the lower light transmission of UV light from 200 to 250 nm indicated that SA/SiO_2 nanocomposite films could potentially be used to prevent lipid damage by UV light in food conservation. © 2016 Wiley Periodicals, Inc. J. Appl. Polym. Sci. **2016**, *133*, 43489.

KEYWORDS: films; mechanical properties; nanoparticles; #nanowires and nanocrystals; polysaccharides; thermogravimetric analysis (TGA)

Received 12 November 2015; accepted 31 January 2016
DOI: 10.1002/app.43489

INTRODUCTION

Edible and biodegradable films from biopolymers, which offer an attractive solution for environmental problems caused by nondegradable plastic packaging materials, have received significant interest from the scientific and industrial communities because of increasing concerns about environmental protection and the use of renewable materials. These biopolymers can be used as an alternative to petroleum-based polymers in film preparation because these materials feature more degradability, nontoxicity, biocompatibility, and reproducibility compared with traditional materials.[1] Alginate has gained considerable attention because of its other fascinating properties, such as its low price, availability, and bioadhesive ability.[2,3] Alginate and alginate-based biocomposites can be readily extracted from the cell wall of brown algae and brown seaweed, and alginate is the only polysaccharide that naturally includes carboxylic groups in every constituent residue.[4,5] Alginate consists of (1–4)-linked β-D-mannuronate (M) acid and α-L-guluronate (G) acid, which can be arranged as mannuronate dyads (MM), guluronate dyads (GG), and heterodyads (MG); the variation of the relative proportion of M units and G units is dependent on the source of alginate in terms of age, species, or part of the brown algae and seaweeds. The most prominent property of alginate is its colloidal property, which allows the formation of an insoluble gel through gelation with calcium cations.[6]

Sodium alginate (SA), which is a water-soluble linear polysaccharide, can be widely used as an adsorbent for ionic dyes,[7] food additives,[8] antibacterial films,[9] wound-healing materials,[10] and stimulus-response drug and releasing materials.[11] In addition, alginate-based biocomposites exhibit a high potential to be further developed for packaging applications. However, these composites lack desired mechanical properties, such as a high

strength, good gas-barrier ability, and water resistance. To improve the mechanical properties of alginate-based biocomposites, scholars have developed various strategies, such as crosslinking,[3] blending with hydrophilic materials (including synthetic or natural polymers),[12,13] and nanoreinforcement to produce nanocomposites. Nano silicon dioxide (nano-SiO_2) particles, which feature a large specific surface area and multiple hydroxyl groups substituted on the surface, can form hydrogen bonds with the polymer matrix. In the past few years, nano-SiO_2 has been used as an additive for organic polymers to improve their mechanical properties, thermal and chemical stability, and water resistance.[14,15] The incorporation of nano-SiO_2 into alginate has been reportedly used for biocatalysts,[16] cell encapsulation,[17] and building blocks[18] by the direct addition of nano-SiO_2 particles or by *in situ* hydrolysis and polycondensation of tetramethoxysilane in alginate solution. However, crosslinked alginate/silicon dioxide (SiO_2) films have not been prepared, and the effects of SiO_2 on the properties and structure of alginate have not been reported in detail. In this study, a tetraethylorthosilicate (TEOS)/ethanol mixture was first combined with a lower concentration of SA solution; the solution pH was regulated to 4 by 0.15 mol/L hydrochloric acid (HCl). Afterward, the alginate power was added step by step to achieve the required concentration. Through this method, nano-SiO_2 could be incorporated well into the alginate solution to obtain the sodium alginate/silicon dioxide (SASI) nanocomposite films. Then, the nanocomposite films were crosslinked by Ca^{2+} to further improve the water resistance. In this study, we aimed to develop an efficient and outstanding material and explore the effect of nano-SiO_2 on the physical and mechanical properties of alginate nanocomposite films.

EXPERIMENTAL

Materials

TEOS [analytical reagent (AR)], HCl (AR), and absolute ethanol (AR) were purchased from Sinopharm Chemical Reagent Co., Ltd. (Shanghai, China). SA (average molecular weight = 2.1×10^6 g/mol) was supplied by Jiejing Seaweed Co., Ltd. (AR, Rizhao, Shandong Province, People's Republic of China). All of the aqueous solutions were prepared with deionized water. All of the glassware was thoroughly cleaned with deionized water and dried in an oven.

Preparation of the Samples

Preparation of the Crosslinking SA Film. SA powder (3.0 g) was added to deionized water (200 mL). The mixture was then stirred vigorously under mechanical agitation (300 rpm) at 60 °C until complete dissolution to produce an SA solution (1.5% w/v). The solution was added to glycerol (25% w/w alginate), and the mixture was stirred for 1 h. Briefly, 55 mL of the solution was cast into Petri dishes ($\varphi = 15$ cm) on a leveled flat surface and allowed to dry in the oven at 40 °C from approximately 8 to 10 h. The dried film was peeled from the Petri dishes and immersed in 30 mL of calcium chloride solution at 5% w/v for 30 min to implement the crosslinking of alginate.

The film was washed with distilled water, and the residual water was removed with filter paper. Before testing, the film was stored in a desiccator with a 52.89% relative humidity over a saturated solution of magnesium nitrate.

Preparation of the SASI Nanocomposite Films by *In Situ* Synthesis. The SA nanocomposite film was prepared through *in situ* synthesis through the following steps. Under mechanical agitation at 40 °C, 1 g of alginate was dissolved in 200 mL of distilled water. The solutions of TEOS/absolute C_2H_5OH (in 4 mol of TEOS) at different ratios were added dropwise to the alginate solution under vigorous agitation. An appropriate quantity of 0.15 *M* HCl was added slowly and continuously to the solution until a pH of 4–5 was reached. The solution was stirred at 60 °C for 2–4 h until it became clear and transparent. Another batch of alginate (2 g) was added to the solution, and the mixture was stirred vigorously at 40 °C for 4 h. Glycerol (in 25% w/w alginate) was then added to the solution; the solution was then agitated at 40 °C for another 1 h. Finally, the nanocomposite solution was degassed for 20 min with an ultrasonicator (Shanghai Kudos SK3300H, China). The solution was then cast into Petri dishes and dried in a thermal oven from 8 to 12 h. The processes of crosslinking and storage were similar to those used to prepare the SA films.

Measurement of the Sample Properties

Film Thickness. The film thickness was measured with a manual digital micrometer (0.01 mm, dial thickness gauge 7301, Mitutoyo Co., Japan). The average value of 10 measurements in different regions of each sample was calculated and was used to determine the mechanical properties, water vapor permeability (WVP), opacity, and light transmittance.

Mechanical Properties. The tensile strength and elongation at break were evaluated at room temperature (23 °C) and at 50% relative humidity with a model WDW-5 microcomputer control electronic universal testing machine (Jide Mechanical Engineering Corp., Jinan, China) according to ASTM D 882. The films were cut into strips (100×15 mm^2) and settled between the tensile grips of the instrument. The initial grip separation was set at 50 mm, and the crosshead speed was set at 1 mm/s. All of the samples were used for triplicate experiments.

Water Content. The water content was measured with a modified method from Galus and Lenart.[19] The cut samples of the films (4×4 cm^2) were dried in air for at least 3 days at a temperature of 20–25 °C and weighed (W_i). Then, they were dried in an oven at 105 °C for 8 h to obtain the finial weight (W_f). The water content was determined in triplicate for each film and was calculated with eq. (1):

$$\text{Water content} = [(W_i - W_f)/W_i] \times 100\% \quad (1)$$

Swelling Degree Test. The swelling degree of the film was determined with the approach reported by Xu *et al.*[20]

Water Solubility Evaluation. The solubility of the films in water was determined by the following steps. The samples were cut in a square (4×4 cm^2) form and then dried at 105 °C for about 8 h to measure the constant weights of the initial dry matter of the films. The samples were then agitated (250 rpm) for 24 h in 50 mL of distilled water at 25 °C. The films were dried again at 105 °C for 8 h to measure their dry weights. Film solubility (%) was calculated with eq. (2):

$$\text{Solubility (\%)} = \frac{\text{Initial dry weight} - \text{Final dry weight}}{\text{Initial dry weight}} \times 100\% \quad (2)$$

The samples were analyzed three times, and the results were expressed as the percentage of solubility of the samples.

WVP. WVP of the films was measured gravimetrically according to the ASTM E 96 desiccant method, as described by Alboofetileh *et al.*[21] Glass permeation cups with an internal diameter of 25 mm and containing distilled water (relative humidity = 100%; vapor pressure at 20 °C = 2.337×10^3 Pa) up to 1.03 cm from the film's underside were covered with the films and then placed in a desiccator. The cups were maintained at 20 °C and 1.5% relative humidity (water vapor pressure = 28.044 Pa) with silica gel under air circulation. The cups were recorded at intervals of 1 h for 8 h. The slope of the weight loss versus time was obtained by linear regression to estimate the water vapor transmission rate. The measured WVP was calculated with eq. (3):

$$\text{WVP} = \frac{\text{WVTR}}{\Delta P} \times L \quad (3)$$

where WVTR is the measured water vapor transmission rate of the cup with the specimen (g m^{-2} s^{-1}), L is the mean film thickness (m), and ΔP is the partial water vapor pressure difference (Pa) between the two sides of the film. This test was repeated three times for each film specimen.

Characterization

X-ray diffraction (XRD; DX2700, China) measurements of the pure SA film and the SASI nanocomposite films were performed with Cu Kα radiation ($\lambda = 1.5418$ Å) at a scan rate (2θ) of 1 °/min at an accelerating voltage of 40 kV and an applied current of 30 mA from 5 to 60 °. The fractured surface morphologies of the alginate/SiO_2 composite film was examined with field emission scanning electron microscopy (SEM; JEOL-7500F, Japan), and the surface elemental analysis of the films was performed with an energy-dispersive spectrometer. The films were frozen in liquid nitrogen and immediately fractured. The fractured surfaces of the films were sputter-coated with platinum to enhance the surface conductivity, and the accelerating voltage was 2 kV. Transmission electron microscopy (TEM) images were obtained with a microscope (Hitachi HT7700) at an accelerating voltage of 100 kV. The composite specimens were prepared by the drop-casting dispersion of nano-SiO_2 within alginate on carbon-coated copper grids, which were dried under ambient conditions. Fourier transform infrared (FTIR) spectroscopy was recorded on a spectrometer (Nicolet 5700), and the spectra were scanned in the range 400–4000 cm^{-1} at a resolution of 4 cm^{-1}. Thermogravimetric analysis was performed with an HCT microcomputer differential thermal balance (Beijing Henwen Scientific Instrument Factory) at a heating speed of 10 °C/min from 25 to 700 °C under air flow (8 mL/min).

Light Transmission and Transparency of the Films

The light transmission and transparency of the pure SA and SASI nanocomposite films were evaluated with a Shimadzu UV3150 UV–visible spectrophotometer according to the method of Norajit *et al.*[8] Samples of the films were cut into rectangular shapes (10×35 mm^2) and then placed in the spectrophotometer cell. The light-barrier properties were determined by scanning of the film samples at wavelengths between 200 and 800 nm with air as a reference. The opacity of the films was calculated with eq. (4):

$$\text{Opacity} = \frac{\text{Abs}_{600}}{x} \quad (4)$$

where Abs_{600} is the absorbance at 600 nm and x is the film thickness (mm). Three samples were measured for each condition.

Surface Color Measurement

The color of the alginate/nano-SiO_2 nanocomposite films was recorded with a color meter (BYK Gardner). The measurements were performed by the placement of the film specimens on a standard white plate [$L^\star = 94.50$, $a^\star = -0.43$, and $b^\star = 1.21$, where the color parameters are $L^\star$ (luminosity), $a^\star$ (red/green), and $b^\star$ (yellow/blue)]. The color difference (ΔE) and whiteness index (WI) were calculated on the basis of the standard plate parameters with eqs. (5) and (6), respectively:

$$\Delta E = \sqrt{(\Delta a^*)^2 + (\Delta b^*)^2 + (\Delta L^*)^2} \quad (5)$$

$$\text{WI} = 100 - \sqrt{(100 - L^*)^2 + (a^*)^2 + (b^*)^2} \quad (6)$$

Statistical Analysis

All of the data are expressed as the means plus or minus the standard deviations. One-way analysis of variance and Duncan's multiple range tests were conducted with SPSS 17 software to identify significant differences among the variables. A value of $p < 0.05$ was considered significant.

RESULTS AND DISCUSSION

SiO_2 Content

The maximum SiO_2 content could not exceed 18 wt % by *in situ* synthesis; otherwise, phase separation occurred, and a uniform and transparent film could not be obtained.

Film Thickness

The films presented thickness values in the range 59.3–51.2 μm. As illustrated in Table I, the composite films' thicknesses decreased after the incorporation of nano-SiO_2. Furthermore, the thickness decreased significantly ($p > 0.05$) at the higher loading level of nano-SiO_2 (12 wt % for the SANI films); this was attributed to the degradation of alginate and the strong interaction of SA and nano-SiO_2.

Mechanical Properties

The mechanical properties (i.e., tensile strength and percentage elongation at break) were examined for the SASI nanocomposite films. These properties were drastically affected by the nano-SiO_2 content (Table I). A previous study showed that the mechanical properties were improved by the interfacial interaction between alginate and nano-SiO_2 [22] For the SANI films, the elongation at break increased significantly ($p < 0.05$) and reached a maximum value of 10.28 ± 0.28 when the nano-SiO_2 content was 6%, and the tensile strength reached a maximum value of 122.2 ± 4.08 MPa when the SiO_2 content was up to

Table I. Effect of SiO_2 on the Film Thickness, Elongation, and Tensile Strength

Sample	Thickness (μm)	Elongation (%)	Tensile strength (MPa)	SiO_2 (wt %)
SA	59.3 ± 0.01^{d}	5.03 ± 0.29^{a}	92.52 ± 3.54^{d}	0
SASI-3	54.0 ± 0.02^{c}	7.84 ± 0.28^{cd}	98.88 ± 7.48^{e}	3
SASI-6	59.2 ± 0.02^{d}	8.40 ± 043^{d}	122.2 ± 4.08^{i}	6
SASI-9	57.8 ± 0.03^{d}	10.28 ± 0.28^{e}	109.67 ± 7.89^{g}	9
SASI-12	52.9 ± 0.02^{bc}	6.53 ± 0.28^{bc}	93.57 ± 2.93^{d}	12
SASI-15	50.6 ± 0.11^{a}	6.33 ± 0.76^{ab}	89.83 ± 2.46^{c}	15
SASI-18	51.2 ± 0.01^{ab}	5.60 ± 0.57^{ab}	87.20 ± 1.77^{b}	18

The data are presented as the means plus or minus the standard deviations. The same superscript letters in the same column indicate no significance between the values ($p > 0.05$). The percentage of SiO_2 was calculated under the assumption that all TEOS was hydrolyzed completely.

9%. This was attributed to the good dispersion of the nanoscale SiO_2 particles in the SA matrix.[23] The decreases in the percentage elongation at break and the tensile strength with a higher content of SiO_2 were caused by the agglomeration and nonuniform dispersion of nano-SiO_2 at high loading values for the self-association of nano-SiO_2. After agglomeration, the nanoparticles lost their nanoeffect, and this resulted in the absence of interfacial interactions between the polymer matrix and nano-SiO_2. The heterogeneous blend could lead to an uneven dispersion of nano-SiO_2 in the nanocomposite films and, thereby, reduced the tensile strength and percentage elongation at break of the nanocomposite film. A similar phenomenon was observed in the polyurethane/SiO_2 nanohybrid membrane.[24]

Water Solubility and Water Content

The water solubility (WS) of SA was determined to measure the water resistance of the SA film sample. WS of the alginate film without crosslinking was $99.55 \pm 0.24\%$;[25] this was almost completely soluble for its highly hydrophilic nature. After crosslinking with Ca^{2+}, WS of the alginate film decreased rapidly to 0.94 ± 0.02 because of the formation of crosslinking between bound calcium ions and carboxyl groups on the surface of the alginate film. Nano-SiO_2 incorporation into alginate matrix decreased its WS from 1.04 ± 0.75 to 2.52 ± 0.96. The results show that the films were practically insoluble after immersion in distilled water for 24 h. Compared with the Ca^{2+} crosslinking alginate films, the WS values of the SASI composite film samples did not significantly change ($p < 0.05$), although the nano-SiO_2 content was lower than 9% (Table II). However, with increasing nano-SiO_2 content to 12–18%, the WS values of the films increased significantly ($p < 0.05$). The reason for that was the reduction of the SA content with the increase in the nano-SiO_2 content, and nano-SiO_2 can solubilize easily in water. Meanwhile, the increase in WS could also be ascribed to the degradation of SA for longer reaction times during the incorporation of nano-SiO_2.[14]

The results in Table II show that the water content of the SA film was 19.42 ± 1.13; this decreased significantly ($p < 0.05$) after the incorporation of nano-SiO_2 exceeded 3 wt %. This was presumably because of the strong interaction between SA and nano-SiO_2. After the incorporation of SiO_2, —OH groups at the surface of SiO_2 could interact with the $—COO^-$ and —OH groups of SA to formulate new H bonds; this decreased the additional active sites for the binding of entering water molecules. A similar result was observed in a study of alginate/cellulose nanocomposite films.[26] The possible mechanisms and performance of the crosslinking of SA and SiO_2 are shown in Scheme 1.

Swelling Degree and WVP

The swelling degree was used as a measure of the extent of crosslinking. Generally, the swelling degree decreases with increasing crosslink density.[3] The swelling degree of the SASI films was dependent on the nano-SiO_2 content, and the swelling degree decreased considerably with decreasing nano-SiO_2 content ($p < 0.05$; Table II). The swelling degree of the SA film was

Table II. Effects of SiO_2 and Different Preparation Methods on the WS, Water Content, Swelling Degree, and WVP Values

Sample	WS (%)	Water content (%)	Swelling degree (%)	WVP ($\times 10^{-10}$ g m m^{-2} Pa^{-1} s^{-1})
SA	0.94 ± 0.02^{a}	19.42 ± 1.13^{f}	108.66 ± 5.34^{j}	0.478 ± 0.005^{d}
SASI-3	1.04 ± 0.75^{ab}	19.34 ± 0.23^{f}	96.35 ± 1.06^{h}	0.407 ± 0.003^{a}
SASI-6	1.06 ± 0.54^{ab}	17.36 ± 0.12^{c}	83.33 ± 0.76^{e}	0.402 ± 0.007^{a}
SASI-9	1.04 ± 0.98^{ab}	18.45 ± 0.87^{e}	72.37 ± 0.23^{d}	0.396 ± 0.010^{a}
SASI-12	2.05 ± 0.65^{c}	17.15 ± 0.11^{b}	60.42 ± 1.54^{a}	0.390 ± 0.002^{a}
SASI-15	2.23 ± 1.04^{d}	17.67 ± 0.14^{d}	67.60 ± 0.67^{c}	0.430 ± 0.011^{b}
SASI-18	2.52 ± 0.96^{e}	16.78 ± 0.21^{a}	65.70 ± 1.86^{b}	0.447 ± 0.011^{c}

The data are presented as the means plus or minus the standard deviations. The same letters in the same column indicate no significance between the values ($p > 0.05$).

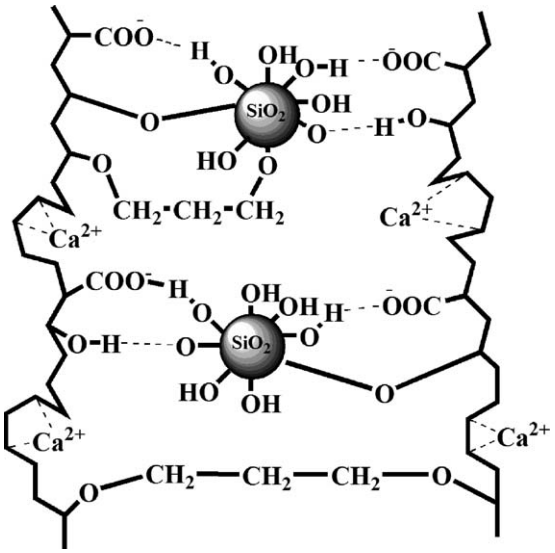

Scheme 1. Possible mechanisms and performance of the crosslinking of SA and SiO_2.

108.66 ± 5.34, whereas the SASI-12 had the lowest swelling degree at about 60.42 ± 1.54. When the nano-SiO_2 content exceeded 12%, the swelling degree of the films increased, but it was still significantly lower than that of the SA film. Nano-SiO_2 addition enhanced the crosslinking density of the films; this was attributed to the hydrogen bonding between the carbonyl groups on the alginate chains and the residual hydroxyls on SiO_2 [25]

Alginate has poor water-vapor-barrier properties because of its high hydrophilicity.[12] The water-vapor-barrier properties of the nanocomposite films were significantly altered with the addition of SiO_2 to the film matrix ($p < 0.05$), as shown by the results in Table II. As such, the WVP properties of the alginate-based films were significantly improved after the addition of the nano-SiO_2 reinforcements. The WVP value of the control film was $0.478 \pm 0.005 \times 10^{-10}$ g m $^{m-2}$ Pa^{-1} s^{-1}. This value was lower than those reported by Rhim.[3] The difference may have been caused by the addition of glycerol and the longer crosslinking time. WVP of the nanocomposite films decreased significantly ($p < 0.05$) by 6.5–18.41%, depending on the SiO_2 concentration. Such a phenomenon of reduction in WVP with the incorporation of SiO_2 was observed with starch/polyvinyl alcohol (PVA).[27] The improvement of the WVP properties of the SiO_2-reinforced alginate films was believed to be caused by the presence of ordered dispersed nano-SiO_2 layers with a large aspect ratio in the SA matrix.[28] They enhanced the roughness of the film, and this resulted in an increase in the effective path length for diffusion of the water molecules to follow a tortuous path through the SA matrix surrounding the SiO_2 particles.[26]

Characterization with XRD, SEM, TEM, and FTIR Spectroscopy

The structures of the SA and SASI nanocomposite films prepared by *in situ* synthesis were verified through XRD analysis, and the results are shown in Figure 1(A), respectively. The amorphous structure of SA was confirmed by the broad diffraction peaks at $2\theta = 14.2°$ of the SA film.[29] However, a new diffraction peak at $2\theta = 22.1°$ was observed in the XRD of the SASI films; this was attributed to the diffraction of amorphous nano-SiO_2 particles.[20] The XRD patterns of the SASI nanocomposite films indicated that the combination with nano-SiO_2 yielded an amorphous structure, whereas the intensity of the peak at $2\theta = 14.2°$ weakened with the increase in the SiO_2 content; this reflected the fact that the crystallinity of alginate was reduced by the addition of SiO_2. For SANI-18, the reflection peak at $2\theta = 14.2°$ disappeared; this showed that the formation of an exfoliated structure for interaction occurred. This became a disagreement that could not be detected by XRD. The results were in agreement with the result of Alboofetileh *et al.*[21] for the incorporation of MMT in an alginate film.

The microdomain structures of the pure alginate and alginate/SiO_2 nanocomposite films were analyzed by FTIR spectroscopy, and the results are shown in Figure 1(B), respectively. The broad absorption band from 3210.13 to 3497.25 cm^{-1} corresponded to the complex stretching vibrations of the

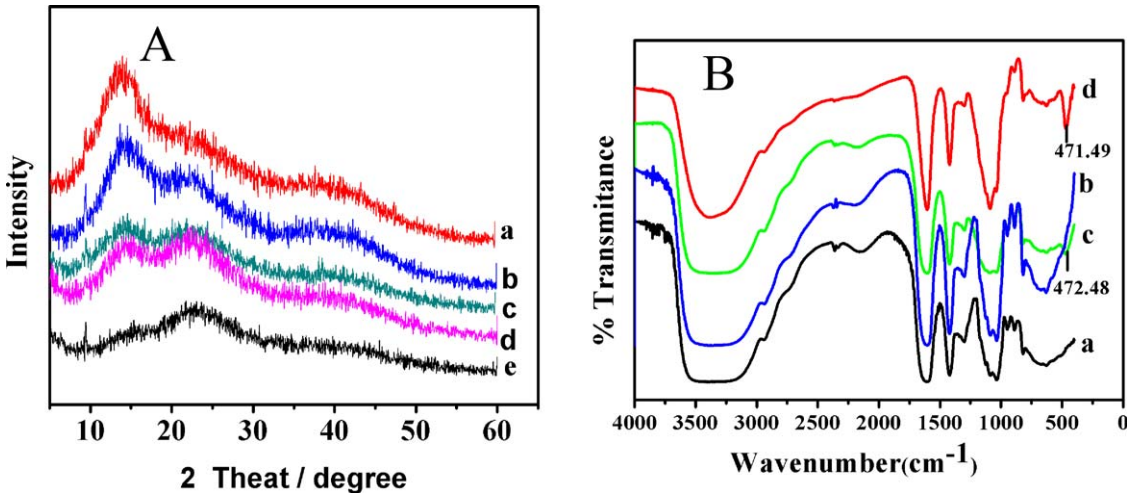

Figure 1. (A) XRD patterns of the SA and SASI films: (a) SA, (b) SASI-3, (c) SASI-6, (d) SASI-12 and (e) SASI-18. (B) FTIR spectra of the SA and SASI films: (a) SA, (b) SASI-3, (c) SASI-9, and (d) SASI-12. [Color figure can be viewed in the online issue, which is available at wileyonlinelibrary.com.]

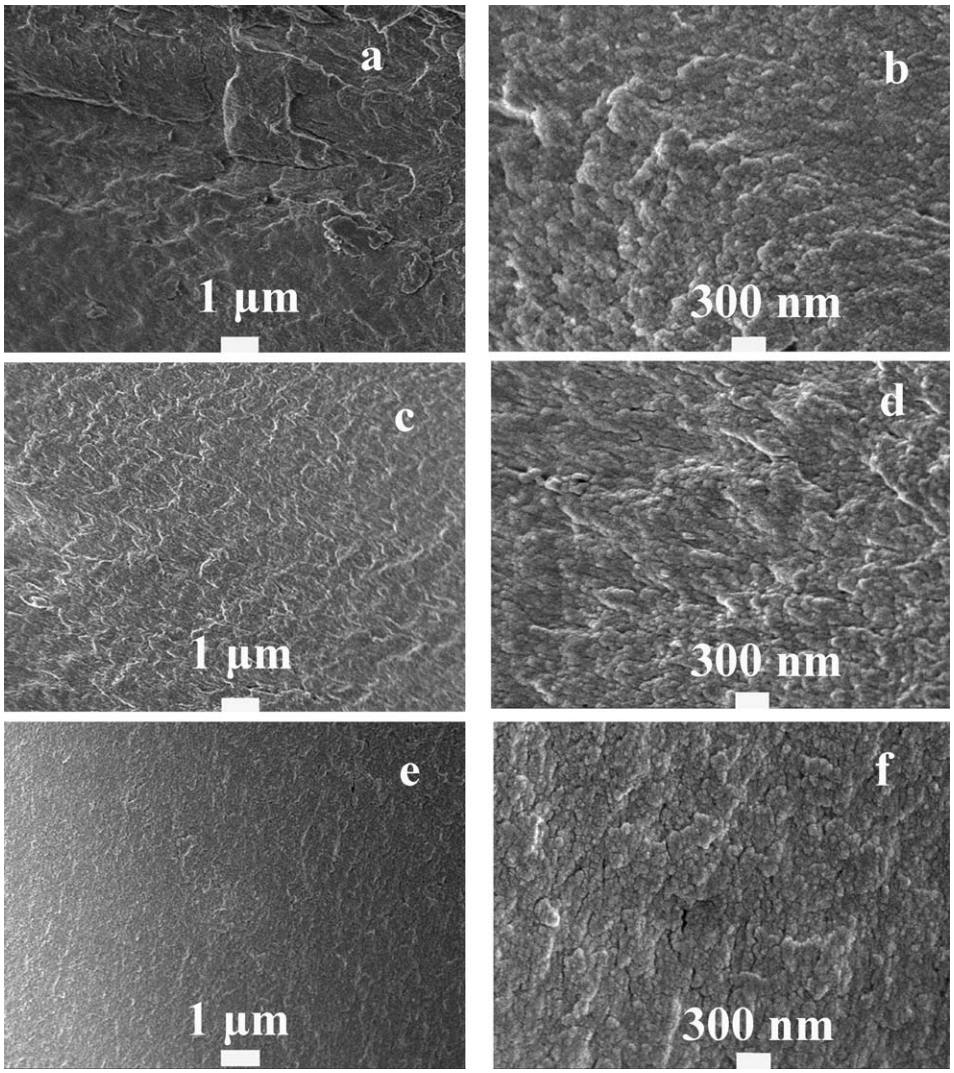

Figure 2. SEM micrographs of the fractured surfaces of the (a,b) SA and (c–f) SASI films: (a) SA, (b) SA magnified, (c) SASI-6, (d) SASI-6 magnified, (e) SASI-18, and (f) SASI-18 magnified.

intramolecular hydrogen bond (intra), the intermolecular hydrogen bond (inter), and free hydrogen bonds, and the absorption bands at 1604.51, 1420.11, and 1035.13 cm^{-1} were relative to the asymmetric and symmetric stretching vibrations of the carbonyl group and the C—O bond of the carboxylate group on the polymeric backbone. The band at 2926.18 cm^{-1} was assigned to the C—H stretching vibrations.[30,31] In addition, new peaks at 472.48 and 471.49 cm^{-1} were observed in the FTIR spectra of SASI-9 and SASI-12, respectively; this demonstrated the formation of Si—O—C bonds between SA and nano-SiO_2,[24,27]

SA and SASI nanocomposite films with different SiO_2 contents were flexible and homogeneous. All of the film samples had relatively smooth surfaces, with no pore or cracks observable by the naked eye. The distribution quality, uniformity of the nanocomposite, presence of voids, agglomeration, and sedimentation of the fractured surface of the SASI composite films were examined by SEM in a more extensive morphological investigation. The morphology of the fractured surface at 10,000 and 30,000 × of the nanocomposite films with 0, 6, and 18% nano-SiO_2 are shown in Figure 2(a–f). All films showed crackled structure; however, the fracture surface of SASI became slightly rougher compared to that of the neat SA film. Figure 2(b–f) also shows that nano-SiO_2 was almost uniformly dispersed in the alginate matrix and that no obvious exfoliation or holes were exhibited. This phenomenon was ascribed to the strong interfacial adherence between the alginate and nano-SiO_2; this was beneficial to the mechanical properties of the nanocomposite films.

The investigation of TEM images (Figure 3) showed that nano-SiO_2 was well dispersed in the alginate matrix, and the diameter of nano-SiO_2 was approximately 20–30 nm for SASI-3 and approximately 100–120 nm for SASI-9.

Analysis of the Thermal Stability

The thermal properties of the pure alginate and SASI nanocomposite films, such as SA, SASI-6, SASI-12, and SASI-18, were studied through thermogravimetric analysis (TGA) under air flow. The TGA results are presented in Figure 4(A).

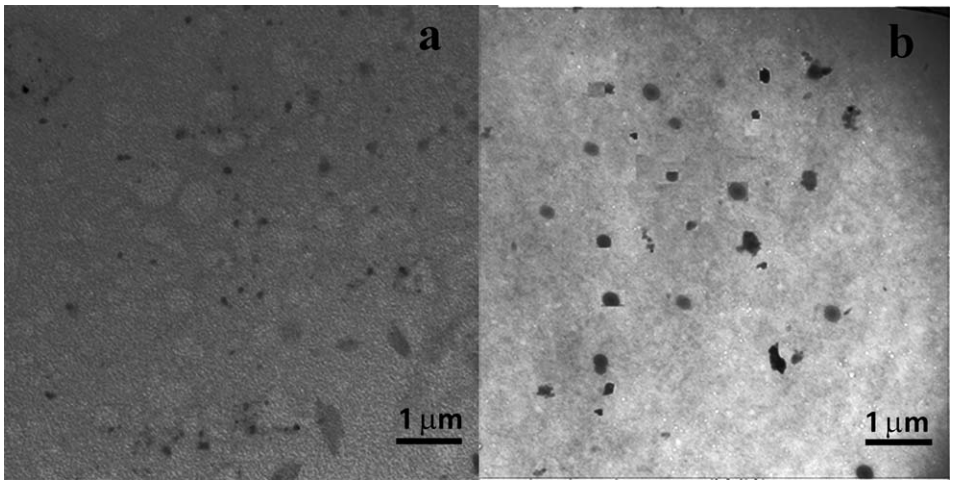

Figure 3. TEM images of the SASI films: (a) SASI-3 and (b) SASI-9.

Nano-SiO_2 considerably influenced the thermal properties of the alginate films, as shown in Figure 4(A), and the thermogravimetry curves revealed that the weight of all of the films decreased in four distinct steps. The first step occurred from 50 to 190 °C and was a consequence of film dehydration. The second step of thermal degradation occurred at 200–280 °C. It was attributed to the thermal destruction of the glycosidic bond and the elimination of the adjacent hydroxyl group and resulted in the formation of the intermediate material.[32,33] The third step occurred at 300–400 °C, during which time the intermediate further decomposed and CO_2 was released simultaneously. The last step occurred at approximately 500 °C, and during this time, the carbonide of the alginate underwent further oxidization and decomposition. Among these four steps, the second step had the most significant effect on the thermal stability of the alginate.[34] The TGA results suggest that nano-SiO_2 helped to increase the thermal stability of the films with decreasing weight of the films and increasing decomposition onset temperature. The decomposition onset temperature of the SA was 52.2 °C; this value shifted to 51.9, 63.9, and 69.9 °C for SASI-6, SASI-12, and SASI-18, respectively. The weight loss of SA was found to be 63.73% at 380 °C, whereas SASI-6, SASI-12, and SASI-18 lost 55.51, 43.71, and 42.77% of their weights, respectively, at the same temperature. The increase in the thermal stability of the SASI nanocomposite films under oxidative atmosphere was attributed to the high thermal stability of nano-SiO_2 compared to that of alginate. As Pu *et al.*[23] reported, the decomposition onset temperatures of the nanocomposites shifted toward a higher temperature scope with increasing inorganic material content. At 700 °C, the thermograms for the films showed 11.92, 12.22, 32.88, and 33.03% residual matter, respectively.

Analysis of the Light Transmission, Opacity, and Color of the Films

The optical properties, including the light transmission and film opacity, were also examined; these parameters significantly affect the appearance of packaged material and are highly important for packaging materials.[35]

The results of the spectroscopic scanning of the SASI nanocomposite films at wavelengths between 200 and 800 nm are shown in Figure 4(B). Although the transmittance of the SASI film determined through UV absorption at wavelengths between 200 and 800 nm decreased slightly with increasing nano-SiO_2 content, the result was higher than that of the pure SA film. Hence, the nanoparticles did not influence the photopermeability. Furthermore, the films containing nano-SiO_2 demonstrated lower light transmissions of UV light from 200 to 250 nm. This

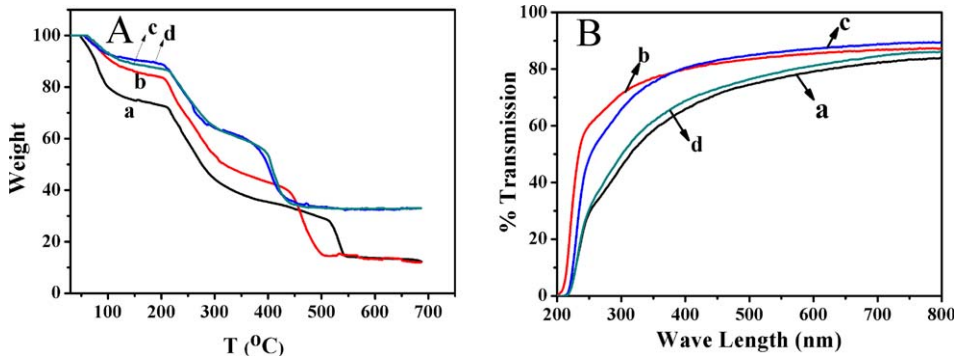

Figure 4. (A) Thermogravimetry curves of the SASI films: (a) SA, (b) SASI-6, (c) SASI-12, and (d) SASI-18. (B) Transmittance (%)–wavelength graph for the SASI films: (a) SA, (b) SASI-3, (c) SASI-9, and (d) SASI-18 (T = temperature). [Color figure can be viewed in the online issue, which is available at wileyonlinelibrary.com.]

Table III. Color Parameter and Opacity Values of the SA and SASI Bionanocomposite Films

Sample	L^*	a^*	b^*	ΔE	WI	Opacity
SA	95.25 ± 0.85^{abc}	-1.39 ± 1.28^{a}	-0.72 ± 0.47^{abc}	2.57 ± 0.49^{abc}	94.87 ± 0.86^{bc}	5.53 ± 0.21^{ab}
SASI-3	93.89 ± 0.21^{a}	0.30 ± 1.02^{ab}	1.04 ± 0.41^{ef}	3.06 ± 0.95^{abc}	93.73 ± 0.28^{ab}	6.31 ± 0.15^{b}
SASI-6	96.16 ± 1.00^{c}	3.11 ± 2.65^{c}	0.88 ± 0.81^{ef}	3.57 ± 1.32^{bc}	94.82 ± 2.49^{bc}	6.23 ± 0.07^{b}
SASI-9	96.36 ± 0.39^{c}	-1.41 ± 0.39^{a}	0.56 ± 1.08^{def}	2.72 ± 0.36^{abc}	95.96 ± 0.51^{c}	8.92 ± 0.15^{c}
SASI-12	95.41 ± 1.24^{bc}	-1.24 ± 0.67^{a}	-0.98 ± 0.34^{bc}	1.29 ± 1.20^{a}	95.14 ± 1.38^{bc}	4.62 ± 0.72^{ab}
SASI-15	96.54 ± 1.11^{c}	$3.1\ 6 \pm 0.77^{c}$	1.46 ± 0.29^{ef}	3.63 ± 0.78^{bc}	95.03 ± 1.00^{bc}	4.45 ± 0.05^{ab}
SASI-18	94.47 ± 0.50^{ab}	1.74 ± 0.90^{bc}	1.92 ± 0.22^{f}	3.75 ± 0.90^{bc}	93.86 ± 0.65^{ab}	3.97 ± 0.15^{a}

The data are presented as the means plus or minus the standard deviations. The same letters in the same column indicate no significance between the values ($p > 0.05$).

finding indicated that alginate films containing nano-SiO_2 could potentially be used to prevent lipid damage by UV light in food conservation.

The opacity values of the alginate/SiO_2 nanocomposite films are presented in Table III. The opacity of the pure alginate film was 5.53; this implied its high transparency. After the addition of nano-SiO_2, the opacity value of the SASI film did not significantly improve, and it decreased when the nano-SiO_2 content exceeded 12%. This indicated that the nano-SiO_2 could have been well dispersed in the SA matrix. The improvement in the transparency have been due to the effect of covalent linkages formed by the tetraethoxysilane groups and the hydrogen bonding between the hydroxyl of SiO_2 and the carboxyl of alginate during hydrolysis.[36] The result for film opacity was consistent with the results of FTIR spectroscopy and SEM.

When an SA film is used as a packaging material, the color properties affects food appearance and consumer approbation, which are important for the packaging industry. The L^*, ΔE, and WI values of the SASI film did not significantly change compared with those of the control film. The color of the film gradually became yellowish and reddish, as the b^* value changed from -0.72 for pure SA to 1.92 and the a^* values changed from -1.39 to 3.16 with increasing nano-SiO_2 content. The WI value of SASI showed that the incorporation of nano-SiO_2 did not change the transparency of the films.[37]

CONCLUSIONS

A number of alginate/SiO_2 nanocomposite films were prepared with glycerol as the plasticizer through *in situ* synthesis. These nanocomposite films were then crosslinked with calcium chloride to obtain crosslinked biocomposite films. The morphology of the fractured surface of the films implied that the nano-SiO_2 dispersed homogeneously in the SA matrix. The tensile strength and elongation of the SASI composite films with 0–18 wt % SiO_2 were improved compared with those of the SA film and reached maximum values at 9 and 6 wt %, respectively. The incorporation of SiO_2 into the composite films reduced the weight loss at 380 °C and improved the residual mass at 700 °C; this indicated that the thermal stability of the composite films was enhanced. On the other hand, the addition of SiO_2 caused reductions in the WVP and swelling degree of the composite films. Furthermore, all of the SiO_2 composite films had a higher transparency than the SA film. Finally, the lower light transmission of UV light from 200 to 250 nm indicated that SASI nanocomposite films can potentially be used to prevent lipid damage by UV light in food conservation.

ACKNOWLEDGMENTS

This work was supported by the Natural Science Foundation of China (contract grant number 51303089) and the Special Fund for Self-Directed Innovation of Shandong Province of China (contract grant number 2013CXB80201).The SEM morphology of the fractured surface was supported by the Qingdao Agriculture University Central Laboratory (Chunhui Hu).

REFERENCES

1. Zohuriaan, M. J.; Shokrolahi, F. *Polym. Test.* **2004**, *23*, 575.
2. Ashikin, W.; Wong, T. W.; Law, C. L. *Carbohydr. Polym.* **2010**, *81*, 104.
3. Rhim, J. W. *LWT Food Sci. Technol.* **2004**, *37*, 323.
4. Ikeda, A.; Takemura, A.; Ono, H. *Carbohydr. Polym.* **2000**, *42*, 421.
5. Lee, K. Y.; Mooney, D. J. *Prog. Polym. Sci.* **2012**, *37*, 106.
6. Johnson, F. A.; Craig, D. Q. M.; Mercer, A. D. *J. Pharm. Pharmacol.* **1997**, *49*, 639.
7. Sui, K. Y.; Li, Y. J.; Liu, R. Z.; Zhang, Y.; Zhao, X.; Liang, H. C.; Xia, Y. Z. *Carbohydr. Polym.* **2012**, *90*, 399.
8. Norajit, K.; Kim, K. M.; Ryu, G. H. *J. Food Eng.* **2010**, *98*, 377.
9. Benavides, S.; Villalobos-Carvajal, R.; Reyes, J. E. *J. Food Eng.* **2012**, *110*, 232.
10. Sikareepaisan, P.; Ruktanonchai, U.; Supaphol, P. *Carbohydr. Polym.* **2011**, *83*, 1457.
11. Mouriñ, V.; Newby, P.; Pishbin, F.; Cattalini, J. P.; Lucangioli, S.; Boccaccini, A. R. *Soft Matter* **2011**, *7*, 6705.
12. Olivas, G. I.; Barbosa-Canovas, G. V. *LWT Food Sci. Technol.* **2008**, *41*, 359.
13. Wang, L.; Auty, M. A. E.; Kerry, J. P. *J. Food Eng.* **2010**, *96*, 199.

14. Gao, X. Y.; Zhu, Y. C.; Zhao, X.; Wang, Z. C.; An, D. M.; Ma, Y. J.; Guan, S.; Du, Y. Y.; Zhou, B. *Appl. Surf. Sci.* **2011**, *257*, 4719.
15. Song, H. Z.; Luo, Z. Q.; Wang, C. Z.; Hao, X. F.; Gao, J. G. *Carbohydr. Polym.* **2013**, *98*, 161.
16. Lu, Y.; Jiang, Z. Y.; Xu, S. W.; Wu, H. *Catal. Today* **2006**, *115*, 263.
17. Gimeno-Fabra, M.; Peroglio, M.; Eglin, D.; Alini, M.; Perry, C. C. *J. Mater. Chem.* **2011**, *21*, 4086.
18. Liu, W. J.; Selomulya, C.; Wu, W. D.; Gengenbach, T. R.; Williams, T.; Chen, X. D. *J. Food Eng.* **2013**, *119*, 299.
19. Galus, S.; Lenart, A. *J. Food Eng.* **2013**, *115*, 459.
20. Xu, J. B.; Bartley, J. P.; Johnson, R. A. *J. Membr. Sci.* **2003**, *218*, 131.
21. Alboofetileh, M.; Rezaei, M.; Hosseini, H.; Abdollahi, M. *J. Food Eng.* **2013**, *117*, 26.
22. Portuga, I.; Dias, V. M.; Duarte, R. F.; Evtuguin, D. V. *J. Phys. Chem. B* **2010**, *114*, 4047.
23. Pu, H. T.; Liu, L.; Chang, Z. H.; Yuan, J. *J. Electrochim. Acta* **2009**, *54*, 7536.
24. Zhou, H.; Chen, Y.; Fan, H. J.; Shi, H.; Luo, Z. Y.; Shi, B. *J. Membr. Sci.* **2008**, *31*, 71.
25. Mason, M. N.; Metters, A. T.; Bowman, C. N.; Anseth, K. S. *Macromolecules* **2001**, *34*, 4630.
26. Abdollahi, M.; Alboofetileh, M.; Behrooz, R.; Rezaei, M.; Miraki, R. *Int. J. Biol. Macromol.* **2013**, *32*, 416.
27. Tang, S. W.; Zou, P.; Xiong, H. G.; Tang, H. L. *Carbohydr. Polym.* **2008**, *72*, 521.
28. Casariego, A.; Souza, B. W. S.; Cerqueira, M. A.; Teixeira, J. A.; Cruz, L.; Diaz, R.; Vicente, A. A. *Food Hydrocolloids* **2009**, *23*, 1895.
29. Bekin, S.; Sarmad, S.; Gürkan, K.; Keceli, G.; Gürdağ, G. *Sens. Actuators B* **2014**, *202*, 878.
30. Yadav, M.; Rhee, K. Y.; Park, S. *J. Carbohydr. Polym.* **2014**, *110*, 18.
31. Pereira, R.; Carvalho, A.; Vaz, D. C.; Gil, M. H. *Int. J. Biol. Macromol.* **2013**, *52*, 221.
32. Soares, J. P.; Santos, J. E.; Chierice, G. O.; Cavalheiro, E. T. G. *Ecl. Quim.* **2004**, *29*, 57.
33. Pongjanyakul, T.; Priprem, A.; Puttipipatkhachorn, S. *J. Controlled Release* **2005**, *107*, 343.
34. Xi, G. X.; Tian, S. J.; Cheng, Q. T.; Zhang, Q. Z. *Chem. World* **2000**, *5*, 254.
35. Pereda, M.; Amica, G.; Racz, I.; Marcovich, N. E. *J. Food Eng.* **2011**, *103*, 76.
36. Kim, S.-K.; Wang, X. W.; Ando, S.; Wang, X. G. *Eur. Polym. J.* **2015**, *24*, 205.
37. Monedero, F. M.; Fabra, M. J.; Talens, P.; Chiralt, A. *J. Food Eng.* **2009**, *91*, 509.